Journal of Non-Crystalline Solids 408 (2015) 102–114

Contents lists available at ScienceDirect

Journal of Non-Crystalline Solids

journal homepage: www.elsevier.com/ locate/ jnoncrysol

# Effects of lithium oxide on the crystallization kinetics of $Na_2O \cdot 2CaO \cdot 3SiO_2$ glass

Leonardo Sant'Ana Gallo [a], Tiago De Marchi Mosca [a], Bruno Henrique Teider [a], Irina Polyakova [b], Ana Candida Martins Rodrigues [a], Edgar Dutra Zanotto [a], Vladimir M. Fokin [c,*]

[a] Vitreous Materials Laboratory, LaMaV-DEMa, Materials Engineering Department, Federal University of São Carlos, P.O. Box 676, São Carlos SP 13565-905, Brazil
[b] Grebenshchikov Institute of Silicate Chemistry, Russian Academy of Sciences, ul. Odoevskogo 24-2, 199155 St. Petersburg, Russia
[c] Vavilov State Optical Institute, ul. Babushkina 36-1, 193171 St. Petersburg, Russia

ARTICLE INFO

*Article history:*
Received 21 August 2014
Received in revised form 18 October 2014
Accepted 20 October 2014
Available online 30 October 2014

*Keywords:*
Glass;
Crystallization;
Nucleation;
Growth

ABSTRACT

The crystal nucleation ($I$) and growth ($U$) rates of $Na_2O \cdot 2CaO \cdot 3SiO_2$ glasses with increasing additions of $Li_2O$ were measured for the primary crystalline phase over wide and overlapping temperature intervals. A partial section of the phase diagram $Na_2O \cdot 2CaO \cdot 3SiO_2$–$Li_2O$ was constructed via DSC analysis and shows a narrow range of solid solution formation that is close to that of $Na_2O \cdot 2CaO \cdot 3SiO_2$. In the four-component system ($Na_2O$–$Li_2O$–$CaO$–$SiO_2$), a pseudo-binary eutectic system of $Na_2O \cdot 2CaO \cdot 3SiO_2$–$Li_2O \cdot SiO_2$ exists. The role of $Li_2O$ in the formation of the crystalline phases was investigated using DSC and X-ray analyses. The addition of $Li_2O$ results in decreases in the glass transition ($T_g$) and liquidus ($T_L$) temperatures. With increasing $Li_2O$ content, both the reduced glass transition temperature $T_{gr}$ ($T_{gr} = T_g/T_L$) and the fragility index, $m$, pass through a minimum. These findings extend and confirm the known inverse correlation between $T_{gr}$ and $I_{max}$ (lower values of $T_{gr}$ correspond to higher values of $I_{max}$) and provide evidence for a similar correlation between $m$ and $I_{max}$. When using the low temperature data for the crystal growth rate ($U$) the viscosity ($\eta$) and diffusivity ($D$) were decoupled at $T < 1.1\ T_g$. Next, a parameter ($U \cdot \eta$ at $T_g$) that characterized the decoupling phenomenon was proposed.


## 1. Introduction

While most fundamental studies of glass crystallization rely on the use of stoichiometric compositions, most commercial glass-ceramics are based on the controlled crystallization of non-stoichiometric glasses, i.e. for which the parent glass composition differs from the crystalline phase [1]. Minor components that are soluble at high temperatures can sometimes precipitate at lower temperatures during the initial stages of phase transformation and form their own crystalline phases. Under some conditions, the latter may serve as an active center for heterogeneous nucleation and the subsequent growth of the main crystalline phase [2–4]. Moreover, soluble additives can affect the crystallization kinetics of the main phase by changing the melt viscosity and its temperature dependence or the free energy of the melt/crystal interfaces [5,6]. For example, small additions of sodium oxide to lithium disilicate glass are known to cause a dramatic decrease (7–8 orders of magnitude) in the internal nucleation rates [7]. A detailed study of nucleation inhibitors for lithium disilicate glass was recently performed in [8].

In contrast, adding relatively small percentages of nucleating agents strongly increases the crystal nucleation rates in glasses. In addition, minor amounts of some foreign components may be incorporated into the structure of the main crystalline phase and form solid solutions. Thus, the possible effects of compositional changes on the pathways and kinetics of crystallization should be systematically investigated from both practical and theoretical standpoints.

In this study, we used a glass with a stoichiometric composition of $Na_2O \cdot 2CaO \cdot 3SiO_2$ ($N_1C_2S_3$), which undergoes spontaneous internal crystallization when properly heated, to study the influence of the addition of $Li_2O$ on its crystallization kinetics. The crystallization kinetics of $N_1C_2S_3$ glass and glasses with similar compositions were investigated in detail (see e.g., [9–12]). The $N_1C_2S_3$ glass belongs to the technologically important sodium–calcium–silicate system, and although this glass is stoichiometric (i.e., an isochemical crystal phase exists), its crystallization follows an unusual pathway. In fact, at deep undercooling ($\sim T_g$), crystallization begins with the homogeneous nucleation of a solid solution that is enriched with sodium relative to the parent (stoichiometric) glass composition [10]. The crystal phase composition only approaches the expected stoichiometry in its more advanced stages of phase transformation. The evolution of the residual glass composition during crystallization is such that it reaches a state in which the refractive indexes of the glass and the crystal phases are similar, which underlies the development of highly crystalline and transparent glass–ceramics with large (micron size) grains [13]. The $N_1C_2S_3$ glass is also employed as a base-glass for bioactive materials [14]. In a cursory study, it was

* Corresponding author.
*E-mail address:* vmfokin@gmail.com (V.M. Fokin).

http://dx.doi.org/10.1016/j.jnoncrysol.2014.10.018
0022-3093/

shown that among several oxide additives only $Li_2O$ accelerates the crystallization kinetics of $N_1C_2S_3$ glass [15]. Therefore, in this paper we return to the preliminary results of [15] to perform a deeper systematic investigation of the crystallization kinetics of $N_1C_2S_3$ glass with different additions of $Li_2O$.

## 2. Materials and methods

Glasses of the following compositions were prepared from analytical grade sodium, calcium (Mallinckrodt), lithium carbonates (Synth) and ground Brazilian quartz (Vitrovita > 99.99% $SiO_2$): $(100\text{-}x)(Na_2O{\cdot}2CaO{\cdot}3SiO_2)xLi_2O$ with x = 1, 2, 3 and 4 wt.%, which correspond to 1.9, 4.3, 5.6, and 7.5 mol% $Li_2O$ and are referred to hereafter as Li-1.9, Li-4.3, Li-5.6 and Li-7.5. The chemicals were thoroughly mixed and melted in a platinum crucible in an electrical furnace at 1450–1500 °C for 2 h before pouring on a steel slab and pressing with a steel plate. The glass compositions are shown in Table 1. The chemical analysis performed for the Li-4.3 and Li-7.5 glasses shows reasonable agreement with the nominal compositions (see e.g., Fig. 1).

The Tammann method was used to estimate the number of crystals per unit volume $N_V(t)$ (the crystal number density) that were nucleated during any given period of time ($t$) at low temperatures $T_n$ close to the glass transition temperature, $T_g$. The nucleated crystals were developed at a higher temperature $T_{dev} > T_n$ up to microscopic sizes (please see details in [16]). After development, the $N_1C_2S_3$ crystals had a spherulitic shape.

Cross sections of the glass samples with developed crystals were prepared for subsequent analyses. A Leica DMRX optical microscope (Leica Microsystems, Wetzlar, Germany) coupled with a Leica DFC490 CCD camera was used to estimate the size and the number densities ($N_V$) of the crystals embedded within the glass interior by using standard stereological methods.

Next, the steady-state nucleation rates and the nucleation time lags were evaluated from the $N_V(t)$ plots. The crystal growth rates, $U$, were estimated as $U(T) = dR/dt$ at the given temperatures, where $R$ is the spherulites radius. In the case of simultaneous nucleation and growth processes with detectable rates, the value of $R$ is related to the largest crystals formed.

A Netzsch 404 differential scanning calorimeter (Netzsch, Selb/Bavaria, Germany) with a platinum crucible was used to analyze the general pathways of the phase transformation, including the crystallization and melting processes, and to estimate the characteristic transformation temperatures. Bulk glass pieces with weights of approximately 30–40 mg were used for the DSC analysis. Heating and cooling were performed at a rate of 10 °C per min.

The viscosities of the studied glasses were estimated using the penetration method.

X-ray diffraction (XRD) measurements were conducted on powdered samples by using a Siemens D5005 (Siemens, Munich, Germany) XRD operating at 40 mA and 40 kV CuKα (λ = 0.15406 nm) used as the incident radiation.

**Table 1**
Glass compositions.

| Glass | $Na_2O$ | CaO | $SiO_2$ | $Li_2O$ |
|---|---|---|---|---|
| | Mol% | | | |
| Li-0[a,b] | 16.4 | 33.3 | 50.3 | |
| Li-1.9 | 16.34 | 32.69 | 49.03 | 1.94 |
| | (16.66) | (33.33) | (50.00) | |
| Li-4.3[a] | 14.8 | 30.2 | 50.7 | 4.3 |
| | (15.5) | (31.6) | (52.9) | |
| Li-5.6 | 15.73 | 31.47 | 47.20 | 5.60 |
| | (16.66) | (33.33) | (50.00) | |
| Li-7.5[a] | 14.8 | 29.0 | 48.7 | 7.5 |
| | (16.0) | (31.3) | (52.7) | |

The values in brackets are recalculated while neglecting lithium oxide.
[a] By analysis.
[b] Taken from [17].

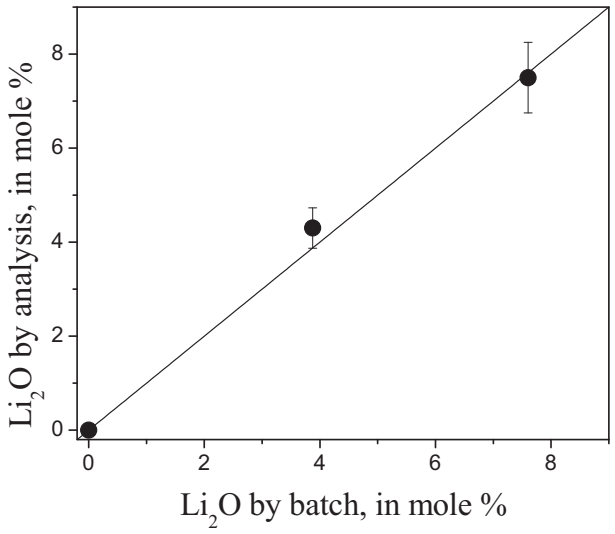


**Fig. 1.** Lithium oxide content by analysis versus synthesis. The line corresponds to the case when the $Li_2O$ content by bath is equal to that by analysis.

## 3. Results

### 3.1. Crystal nucleation

Some examples of the dependency of the crystal number density ($N_V$) on time in the Li-4.3, Li-5.6, and Li-7.5 glasses are shown in Fig. 2 for several temperatures. The solid lines were plotted by using Eq. (1) for the time-dependency of the number of super-critical nuclei (see e.g. [2]).

$$N_V(t) = I_{st}\tau\left(\frac{t}{\tau} - \frac{\pi^2}{6} - 2\sum_{m=1}^{\infty}\frac{(-1)^m}{m^2}\exp\left(-m^2\frac{t}{\tau}\right)\right). \quad (1)$$

This equation includes two fundamental parameters that can be estimated as fit parameters, the steady-state nucleation rate ($I_{st}$) and the time lag for nucleation ($\tau$). The temperature dependencies of $I_{st}$ and $\tau$ are shown in Figs. 3 and 4, respectively. The data for the Li-0 glass were obtained from [17]. The arrows in Fig. 3 denote the values of the glass transition temperatures that were obtained from the DSC heating curves.

### 3.2. Crystal growth

Fig. 5 shows an example of the time dependency of the crystal size at two temperatures that were used for determining the crystal growth rates in the Li-7.5 glass. The temperature dependencies of the crystal growth rates (log ($U$)) are presented in usual and Arrhenius coordinates (inset) as shown in Fig. 6 for the Li-0, Li-4.3, Li-5.6, and Li-7.5 glasses. The growth data for the Li-0 glass were obtained from [17]. The temperature interval of the crystal growth measurements overlaps with the interval that was used for estimating the nucleation rates (please compare Figs. 6 and 3). In fact, for the Li-7.5 glass, the temperature interval includes the glass transition temperature.

### 3.3. Viscosity

The temperature dependences of the viscosities are shown in Fig. 7 for the Li-0, Li-1.9, Li-4.3, Li-5.6, and Li-7.5 glasses. The measurements for the Li-1.9, Li-4.3, Li-5.6, and Li-7.5 glasses were kindly performed by V.P. Klyev, who used the penetration method. The lines were plotted

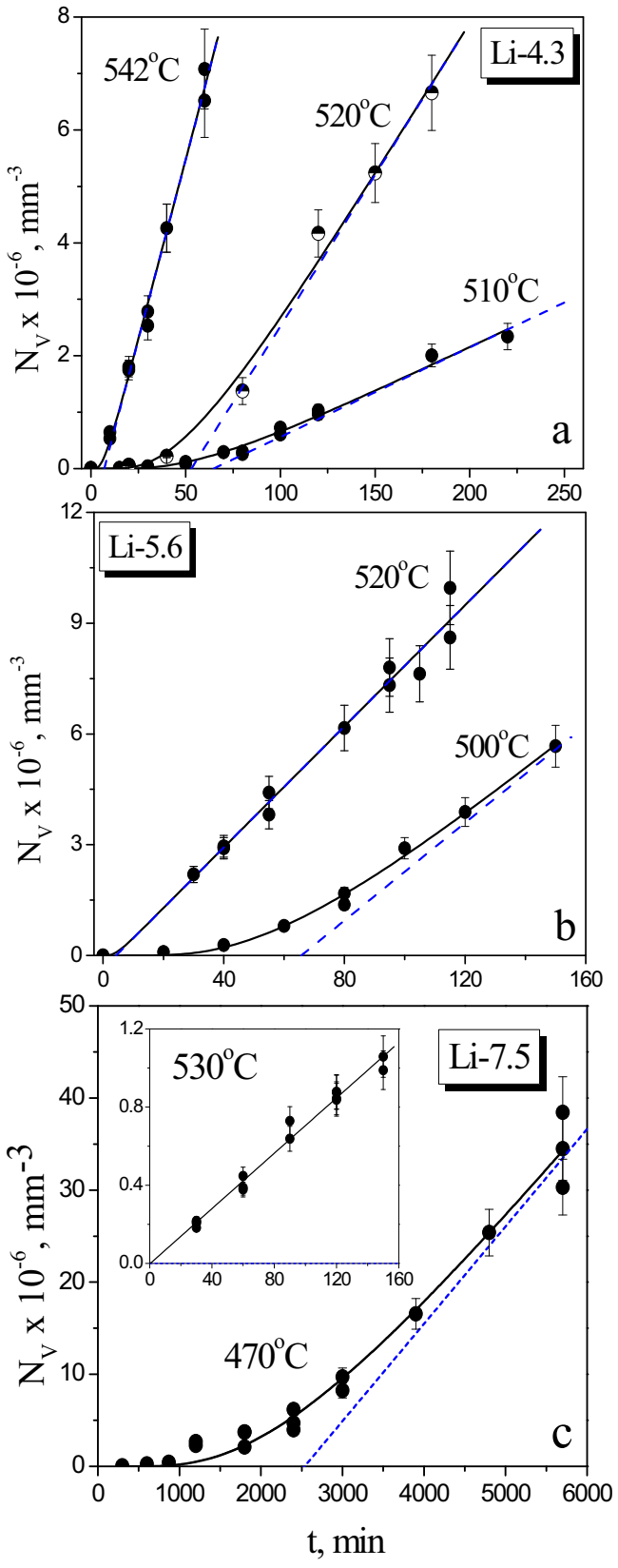


**Fig. 2.** Crystal number densities versus the time of nucleation at several temperatures in the Li-4.5 (a), Li-5,6 (b), and Li-7.5 (c) glasses. The solid lines are plotted by Eq. (1), and the dashed lines are the proper asymptotes.

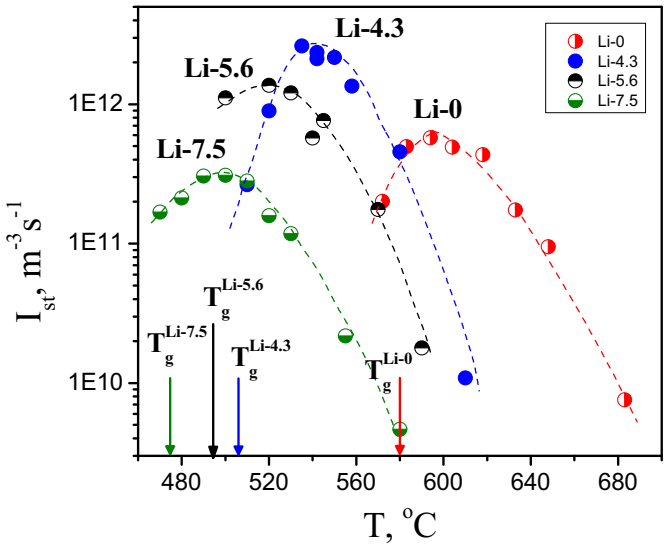


**Fig. 3.** The steady state nucleation rates versus temperature for the different glasses. The arrows show the glass transition temperatures. Data for Li-0 glass were obtained from [17].

by using the Vogel–Fulcher–Tammann (VFT) Eq. (2) with parameters of $A$, $B$, and $T_o$ estimated as fitting parameters, which are listed in Table 2.

$$\log\eta = A + \frac{B}{T - T_o} \tag{2}$$

The solid lines correspond to the intervals of the viscosity measurements. These intervals are relatively narrow and only relate to the high values of viscosity. It may be the cause of the unusual values of the A parameters for glasses Li-1.9 and Li-1.4 on Table 1. Therefore, we only used these fit parameters for the analysis of the viscosity near the glass transition temperature, which was similar to the temperature interval of the crystallization measurements.

### 3.4. Thermo analysis

Fig. 8 shows the DSC heating and cooling curves for the bulk glass. In addition, several characteristic temperatures, the glass transition

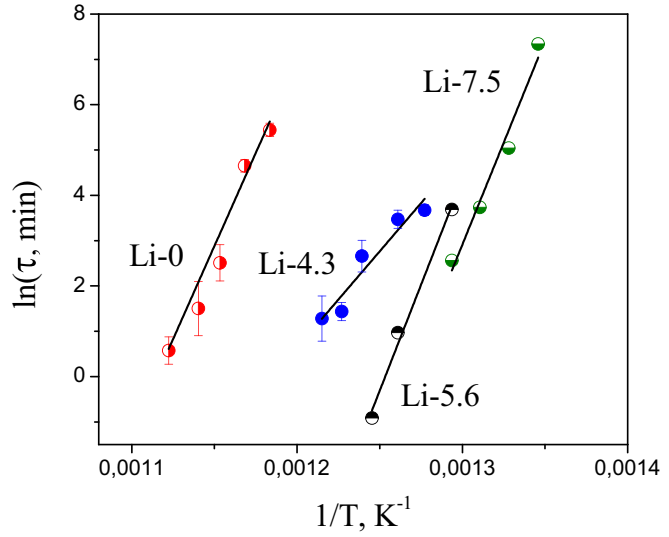


**Fig. 4.** Nucleation time-lag versus the inverse temperatures for the different glasses. Data for Li-0 glass were obtained from [17].

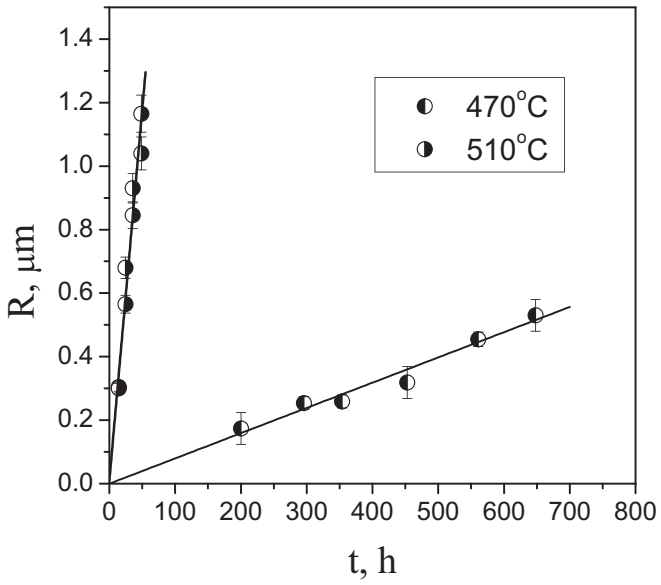


**Fig. 5.** Radius of the 1N2C3S crystals in Li-7.5 glass versus time of growth at 470 °C and 510 °C.

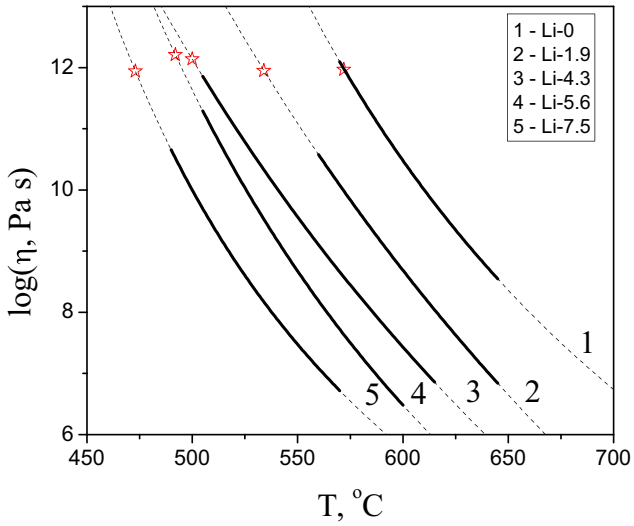


**Fig. 7.** Viscosity versus temperature for the different glasses. The lines are plotted according to the VFT equation with the parameters collected in Table 2. The solid portions of the lines correspond to the measured temperature interval. The stars show the glass transition temperatures that were estimated from the DSC heating curves.

temperature ($T_g$), the solidus ($T_S$), liquidus ($T_L$), and the temperature of the polymorphic transition ($T_{pm}$) are shown.

### 3.5. X-ray phase analysis

Fig. 9 shows the X-ray diffraction spectra of the Li-0, Li-1.9, Li-4.3, Li-5.6, and Li-7.5 glasses, which were previously crystallized over 30 min at the temperatures just after the respective crystallization peaks in the DSC heating curves (see Fig. 8).

## 4. Discussion

The main topics of this research include i) the non-monotonic and monotonic evolutions of the nucleation and growth rates, respectively, with increasing $Li_2O$ content; ii) the influences of $Li_2O$ on the melt viscosity and its fragility; and iii) the role of $Li_2O$ in the formation of the crystal phase.

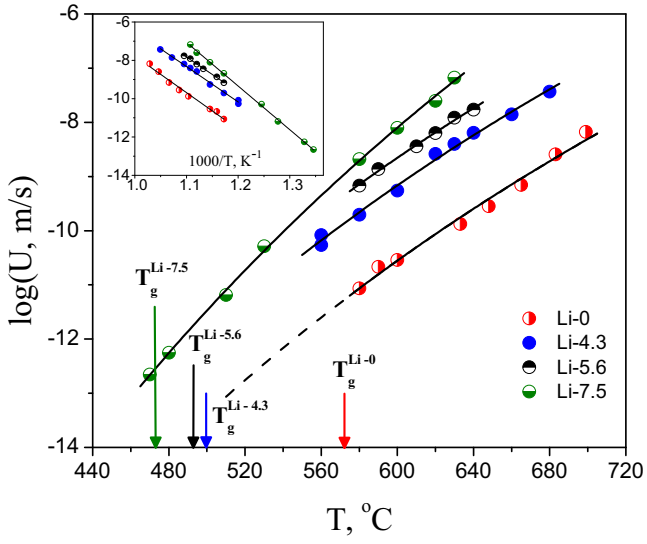


**Fig. 6.** Crystal growth rates versus temperature for the different glasses. The arrows show the glass transition temperatures. The inset shows the same data in Arrhenius coordinates. Data for Li-0 glass were obtained from [17].

### 4.1. Main equations

The analysis of the crystallization kinetics (nucleation rates and crystal growth rates) was performed in the framework of the classical nucleation theory (CNT) and the screw dislocation growth model. The main equations are shown below.

#### 4.1.1. Nucleation rate

According to CNT, the steady state nucleation rate can be written as follows [2]:

$$I_{st} = I_o \exp\left[-\frac{W_* + \Delta G_D}{k_B T}\right], \quad (3)$$

with

$$W_* = K\frac{\sigma^3}{\Delta G_V{}^2}, \text{ and}$$

$$I_o = 2N_1\frac{k_B T}{h}\left(\frac{a^2\sigma}{k_B T}\right)^{1/2},$$

where $W_*$ is the *thermodynamic barrier* for nucleation (i.e., the increase in the free energy of a system due to the formation of a nucleus with a critical size), σ is the specific surface free energy of the critical nucleus/melt interface, $K$ is the shape factor, which is equal to 16π/3 in the case of a spherical nucleus, and $\Delta G_V$ is the difference between the free energies of the liquid and crystal per unit volume of the crystal (i.e., the

**Table 2**
Parameters of the VFT equation for viscosity in Pa·s.

| Glass | A | B, K | $T_o$, K |
|---|---|---|---|
| Li-0 | −5.46 | 5196 | 547 |
| Li-1.9 | −17.98 | 16,132 | 268 |
| Li-4.3 | −15.13 | 13,058 | 294 |
| Li-5.6 | −8.16 | 5628 | 489 |
| Li-7.5 | −3.01 | 2702 | 565 |

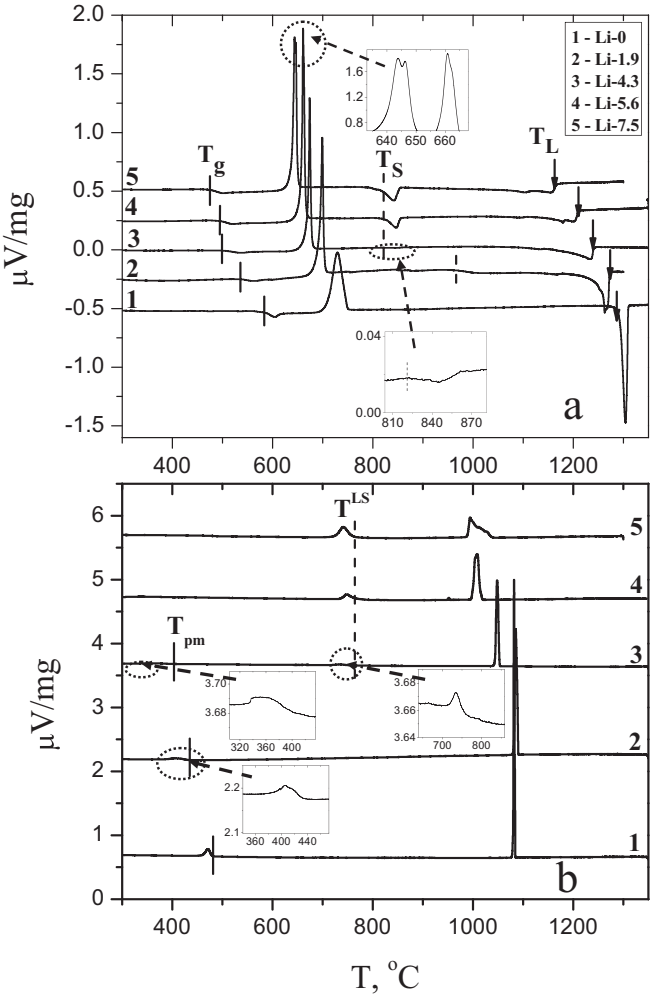


**Fig. 8.** The DSC heating (a) and cooling (b) curves for the different glasses obtained for the heating/cooling rates |C| = 10 °C/min.

thermodynamic driving force for crystallization). In addition, $N_1 \approx 1/a^3$ is the number density of the "structural units" with a size of $a$ that is involved in the formation of the crystal phase and $\Delta G_D$ is the *kinetic barrier*

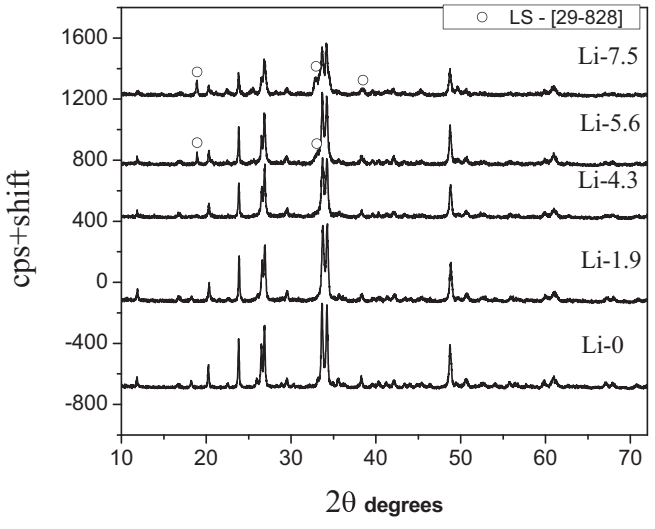


**Fig. 9.** X-ray diffraction pattern of the fully crystallized glasses at temperatures just after the DSC exothermic crystallization peak. Unmarked peaks correspond to $N_1C_2S_3$.

(i.e., the activation free energy for the transfer of a 'structural unit' from the melt to a crystal nucleus), which determines the effective diffusion coefficient $D$.

$$D = \frac{k_B T}{h} a^2 \exp\left(-\frac{\Delta G_D}{k_B T}\right) \tag{4}$$

Here, $k_B$ and $h$ are the Boltzmann and Planck constants, respectively. The pre-exponential term in Eq. (3) ($I_o$) depends weakly on the temperature when compared with the exponential function.

In this study, we used the following equation for the thermodynamic driving force ($\Delta G_V$), which was derived in [18] for binary (metallic) melts:

$$\Delta G_V = (T_L - T)(\Delta S_m - R \ln x)/V_m, \tag{5}$$

where $T_L$ is the liquidus temperature, $\Delta S_m$ is the entropy of fusion per mole of the pure crystal, $x$ is the molar fraction of the precipitating substance in the melt and $V_m$ is its molar volume. In our case, $x$ is related to the main crystalline phase ($Na_2O{\cdot}2CaO{\cdot}3SiO_2$) for which the nucleation rates were estimated. It should be noted that when $x = 1$ (stoichiometric crystallization), Eq. (5) is transformed into the well-known Turnbull equation [2]. Strictly speaking, $x$ should be introduced into the pre-exponential term of Eq. (3) to account for the decrease in the number of structural units that participate in the nucleation of the new phase relative to the stoichiometric crystallization. However, in our case, this factor is weak and can be neglected. In addition, when using Eq. (5), we neglected the solubility of Li in the $Na_2O{\cdot}2CaO{\cdot}3SiO_2$ crystals (see Section 4.4) and assumed that most of the $Li_2O$ remained in the undercooled liquid phase, at least during the nucleation stage.

The time scale parameter, $\tau$ (see Eq. (1)), for the establishment of the steady state nucleation rate ($I_{st}$) is commonly denoted as the time-lag for nucleation and can be written as follows [19]:

$$\tau = \frac{16}{\pi^2} \frac{h\sigma}{\Delta G_V^2 a^4} \exp\left(\frac{\Delta G_D}{k_B T}\right) \tag{6}$$

By combining Eqs. (3) and (6), one can write the following equation for the steady-state nucleation rate:

$$I_{st} = \frac{32}{\pi^2} \frac{k_B^{1/2} \sigma^{3/2}}{a^6} \frac{T^{1/2}}{\Delta G_V^2 \tau} \exp\left[-\frac{W_*}{k_B T}\right]. \tag{7}$$

For a first approximation, the shear viscosity ($\eta$) is often used to estimate the kinetic barrier by assuming that the free activation energy of the viscous flow ($\Delta G_\eta$) in Eq. (8) [20] is equal to $\Delta G_D$

$$\eta = \frac{k_B T}{a^3} \tau_o \exp\left(\frac{\Delta G_\eta}{kT}\right), \tau_o = h/k_B T, \tag{8}$$

where $\tau_o$ is a characteristic time of the order of the period of atomic vibration and is estimated at approximately $10^{-13}$ s. Under the above assumption ($\Delta G_D = \Delta G_\eta$), the combination of Eqs. (8) and (3) gives

$$I_{st} = \frac{1}{2} \frac{k_B^{1/2} \sigma^{1/2}}{a^5} \frac{T^{1/2}}{\eta} \exp\left[-\frac{W_*}{k_B T}\right]. \tag{9}$$

Eq. (9) supposes the validity of the Stokes–Einstein–Eyring Eq. (10).

$$D_\eta = \frac{k_B T}{a\eta} \tag{10}$$

*4.1.2. Growth rate*

According to Jackson's treatment of the interface [21], the materials with a high melting entropy (>4$R$) are expected to exhibit crystal growth kinetics that are predicted by either the screw dislocation or

the 2D surface nucleation growth models. The melting entropy ($\Delta S_m$) of the main crystalline phase, $Na_2O{\cdot}2CaO{\cdot}3SiO_2$, is $7R$ [22]. Because the choice from the above two models does not affect the result of the analysis performed in Section 4.3, we will use the screw dislocation model because it is the simplest. According to this model, the crystal growth rate ($U$) can be written as follows [2]:

$$U = f\frac{D_U}{4a}\left[1-\exp\left(-\frac{1}{2}\frac{\Delta G_V a^3}{k_B T}\right)\right] \text{ with } f\approx\frac{1}{2\pi}\frac{T_L-T}{T_L}, \quad (11)$$

where $f$ is the fraction of the preferred growth sites at the interface (i.e., the dislocation edges).

By assuming that $D_U = D_\eta$, Eq. (11) can be rewritten as follows:

$$U = f\frac{k_B T}{4a^2\eta}\left[1-\exp\left(-\frac{1}{2}\frac{\Delta G_V a^3}{k_B T}\right)\right] \quad (12)$$

### 4.2. Nucleation rate versus $Li_2O$ content

From Fig. 3, the first addition of lithium oxide to the $Na_2O{\cdot}2CaO{\cdot}3SiO_2$ glass resulted in an increase in the maximum steady-state nucleation rate, $I_{max} \equiv I_{st}(T'_{max})$ (please compare the Li-0 and Li-4.3 glasses), which corresponded with the results of [14]. The subsequent increase in the $Li_2O$ content resulted in a decrease in the $I_{max}$. Thus, the influence of $Li_2O$ on the nucleation rate is non-monotonic and reveals a maximum at some $Li_2O$ concentration. Fig. 10 shows the reduced sum of the nucleation barriers ($W_* + \Delta G_D$), which was estimated from the experimental values of $I_{st}$ (see Fig. 3) via Eq. (3), versus the temperature. To evaluate $I_o$, we used $\sigma = 0.12$ J/m$^2$ [23] and $a \approx (V_m/N_A)^{1/3} = 7.5\times10^{-10}$ m ($V_m$ is the molar volume and $N_A$ is Avogadro's number). The pre-exponential term, $I_o$, only depends weakly on temperature, if compared to the exponential function, and varies between $10^{41}$ and $10^{43}$ m$^{-3}{\cdot}$s$^{-1}$ for the different condensed systems [24]. Hence, the arbitrary natures of the employed parameters $a$ and $\sigma$ do not strongly affect the final result. Interplay between the thermodynamic and kinetic barriers (the decrease of the former and the increase of the latter with decreasing temperature) results in the temperature maximum of the nucleation rate (minimum of $(W_* + \Delta G_D)/k_BT$). The temperature of the maximum nucleation rate ($T'_{max}$) is determined from the condition of equality between the absolute values of the temperature derivatives of $W_*$ and $\Delta G_D$. $T'_{max}$ is normally near the glass transition temperature. This experimental fact underlies the following trend: the lower the reduced glass transition temperature ($T_{gr} = T_g/T_L$), the higher the undercooling achieved at $T_g$, and the higher the maximum nucleation rate $I_{max} = I_{st}(T'_{max} \approx T_g)$ [5] due to the increased thermodynamic driving force $\Delta G_V(T_g)$, which increases with undercooling. The above definition of $T_{gr}$ is related to the primary crystallizing phase, in our case $Na_2O{\cdot}2CaO{\cdot}3SiO_2$. At constant pressure, the variation of $T_{gr}$ can only be realized by changing the glass composition. Generally, such variation is accompanied by smaller or larger changes in the other parameters that affect the nucleation rate. Therefore, to observe the trend discussed above, one must collect a plethora of nucleation data or select data for nucleation of the same crystals in glasses with similar compositions. A detailed analysis of the correlations between $I_{max}$ and $T_{gr}$ may be found in [5].

Fig. 11 shows the $I_{max}$ (a) and $T_{gr}$ (b) values as a function of the $Li_2O$ content. The value of $T_{gr}$ passes through a minimum at a $Li_2O$ concentration of 4 mol%, which is near the composition of the Li-4.3 glass that reveals the highest $I_{max}$ value. Thus, we may assume that the highest value of $I_{max}$ mainly results from the lowest value of $T_{gr}$ for this series of glasses. Fig. 12 shows the $I_{max}$ (a) and $T'_{max}$ (c) data for the $N_1C_2S_3$ glasses with different $Li_2O$ contents as a function of the reduced glass transition temperature. The same data are plotted in Fig. 12b and d

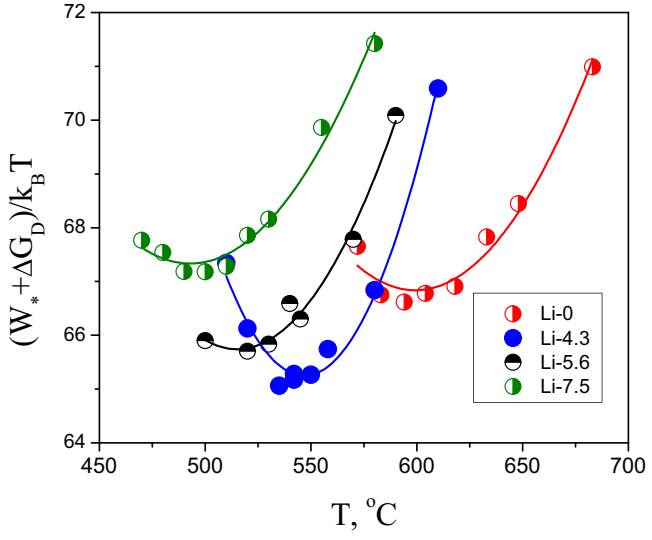


**Fig. 10.** Sum of the thermodynamic and kinetic barriers versus temperature for glasses with different $Li_2O$ contents.

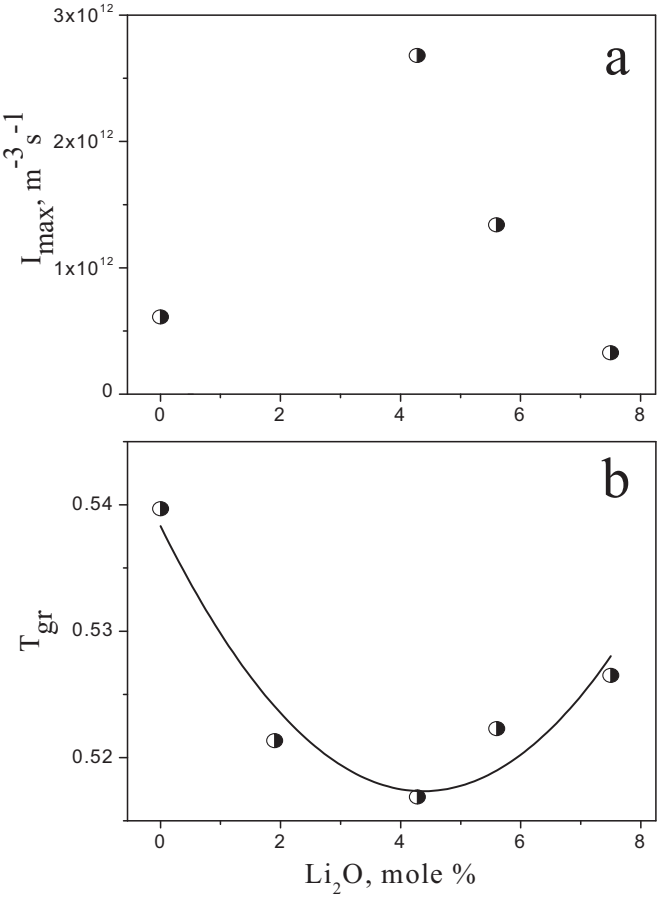


**Fig. 11.** $I_{max}$ (a) and $T_{gr} = T_g/T_L$ (b) versus $Li_2O$ content. The values of $T_g$ and $T_L$ were taken from the DSC curves (see Fig. 8). The line is a guide to the eyes.

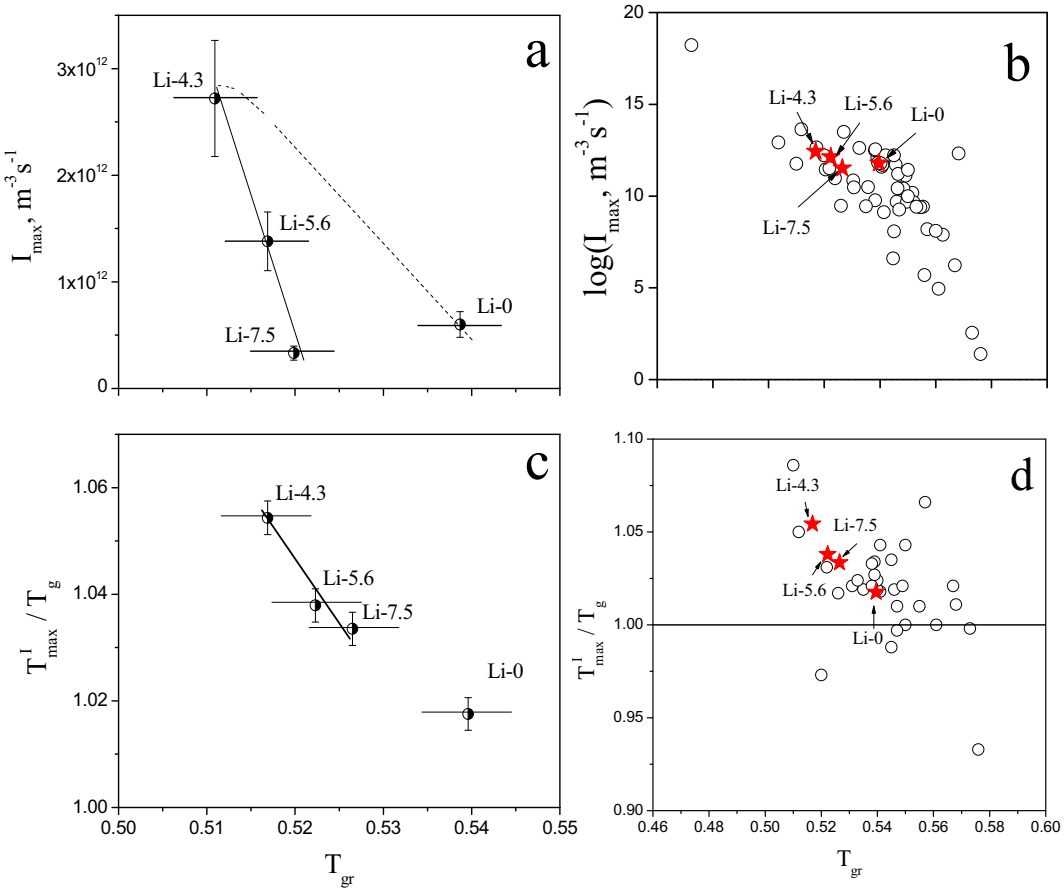


**Fig. 12.** $I_{max}$ (a, b) and reduced temperature $T^I_{max}/T_g$ (c, d) versus the reduced glass transition temperature $T_{gr}$ for the Li-0, Li-4.3, Li-5.6, and Li-7.5 glasses. For the purpose of comparison, panels b and d present data for several glasses that are taken from [5]. The line is included as a guide to the eye.

with a variety of other data for several glasses taken from [5]. To demonstrate the correlation between $I_{max}$ and $T_{gr}$, we used data from the Li-4.3, Li-5.6, and Li-7.5 glasses, for which the $T_{gr}$ values increased as the $Li_2O$ content increased (see Fig. 11b). The $I_{max}$ for these glasses decreased as the $T_{gr}$ (Fig. 12a) increased, which corresponded with the general trend shown in Fig. 12b. Despite the absence of nucleation data for the glasses containing $Li_2O$ between 0 to 4.3 mol%, it is clear that the maximum nucleation rates must increase in this compositional interval, as schematically shown by the dashed line in Fig. 12a.

Fig. 12c shows one more correlation: the higher is the reduced glass transition temperature $T_{gr}$, the closer is the temperature of maximum nucleation rate $T^I_{max}$ to the glass transition temperature $T_g$ (the $T^I_{max}/T_g$ ratio becomes closer to one). This trend agrees with the results for several glasses that were collected in [5] (see Fig. 12d). Thus, $Li_2O$ mainly affects the nucleation rate by altering the reduced glass transition temperature because both the $T_L$ and $T_g$ vary.

A correlation between the maximum crystal growth rate $U_{max} = U(T^U_{max})$ and the $T_{gr}$ (the lower the reduced glass transition temperature, the higher the maximum crystal growth rate) was also demonstrated for different glass-forming systems including not only oxides [25] but also organics, chalcogenides, and metals [26]. However, this correlation is much weaker than that for the nucleation rate. In addition, it must be remembered that $T^I_{max} << T^U_{max}$ because the former is closer to $T_g$ and the latter is closer to $T_L(T_S)$. The growth rates presented in this study are related to low temperatures that are far from the $T^U_{max}$ (high undercooling) and are mainly determined by the effective diffusion coefficient (see Eq. (12)), which increases monotonically as the $Li_2O$ content increases.

Another unexpected correlation is shown in Fig. 13. Fig. 13 shows the relationship between the fragility index ($m$) that was estimated by Eq. (13) [27] and the reduced glass transition temperature ($T_{gr}$).

$$m = \left.\frac{d(\log_{10}\eta)}{d\left(T_g/T\right)}\right|_{T=T_g} \tag{13}$$

Generally, $T_{12}$ (the temperature corresponding to the viscosity of $\eta = 10^{12}$ Pa·s) is used instead of $T_g$. This approximation is rather consistent, as shown in Fig. 14.

According to Fig. 13, the dependencies of both $m$ and $T_{gr}$ on the $Li_2O$ content reveal a minimum for the Li-4.3 glass. The Li-4.3 glass has the highest maximum nucleation rate ($I_{max}$). At first glance, the fragility is not connected with the crystallization kinetics because it does not include the temperature of the liquidus and the undercooling that determines the thermodynamic driving force for crystallization. However, as previously mentioned, the temperature of the maximum nucleation rate ($T^I_{max}$) is determined by the conditions of equality between the absolute values of the temperature derivatives of $W_*$ and $\Delta G_D$. The fragility index reflects the variation of viscosity with temperature near the $T_g$, (i.e., close to $T^I_{max}$), being equal to the reduced activation enthalpy of viscous flow. Replacing $\Delta G_D$ by the activation energy of viscous flow, $\Delta G_\eta$, as done in Eq. (9), we can suppose that the lower is $m$ the lower temperature at which the conditions for $I_{max}$ is achieved. A decrease in the $T^I_{max}$ is accompanied by a decrease in the thermodynamic barrier for nucleation [16]. However, in every special case

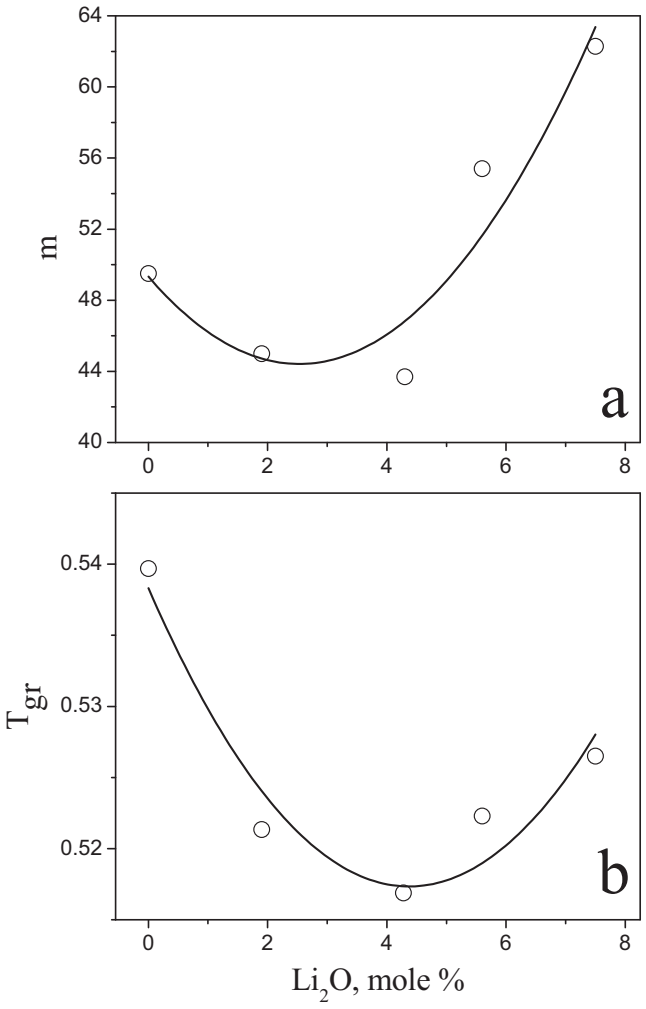


**Fig. 13.** Fragility index (a) and the reduced glass transition temperature (b) versus the $Li_2O$ content in the parent glasses. The line is included as a guide to the eye.

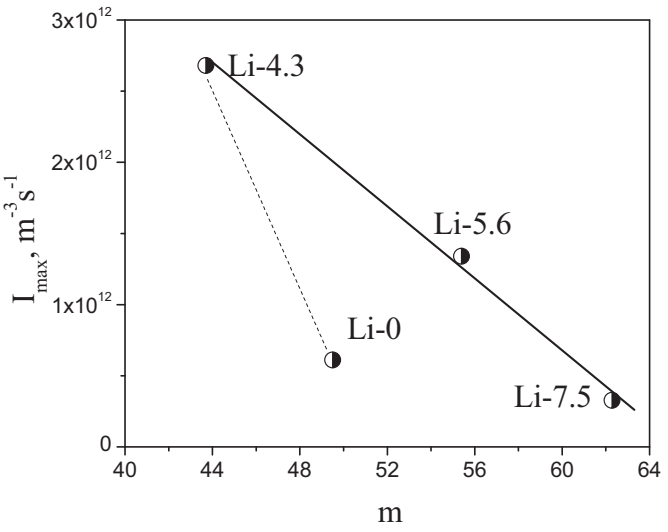


**Fig. 15.** Maximum nucleation rates versus the fragility index. The lines are included as a guide to the eye.

one has to take into account not only the variation of the temperature dependence of viscosity but also its absolute value. For our case, according to Fig. 15, lower fragility indexes ($m$) correspond with higher $I_{max}$ values. Similar to Fig. 12a, the dependence of $I_{max}$ on $m$ in the full composition range (Li-0–Li-7.5) exhibits a kink-like shape because two glass compositions correspond to just one value of $m$. This kink also demonstrates the dependence of $m$ on $T_{gr}$ (Fig. 16). In light of the problem discussed above, it is desirable to study the crystallization kinetics in the glasses with compositions between those of Li-0 and Li-4.3.

In his recent review entitled "Early stages of crystal formation in glass-forming metallic alloys", G. Wilde [28] concluded that the fragility index does not provide a suitable criterion for metallic glass-forming systems because the large range of critical cooling rates for metallic alloys (approximately 8 orders of magnitude) is not accompanied by a significant change in the fragility parameter ($35 < m < 55$). Here the following comment could be made: the critical cooling rate mainly reflects the kinetics of the overall crystallization process rather than only the nucleation rate. However, our data refer to the maximum

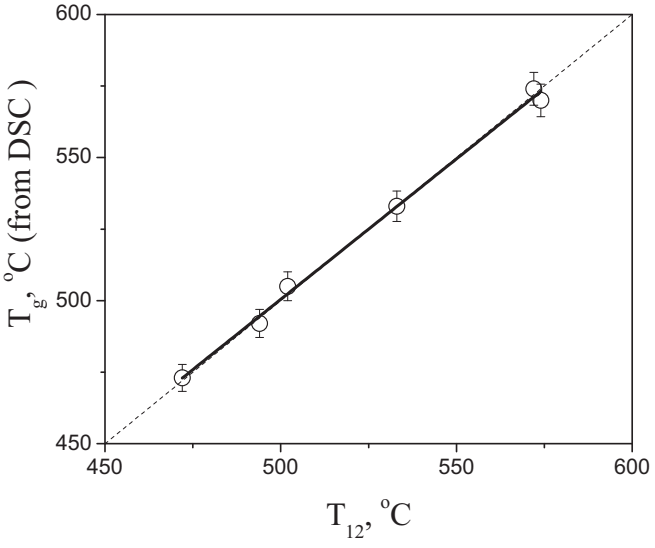


**Fig. 14.** Correlation between $T_{12}$ and $T_g$, which was estimated from the DSC heating curves with a heating rate of 10 °C/min for the $Na_2O{\cdot}2CaO{\cdot}3SiO_2$ glasses with and without $Li_2O$. The solid line is a linear fit, and dashed line corresponds to the condition of $T_g = T_{12}$.

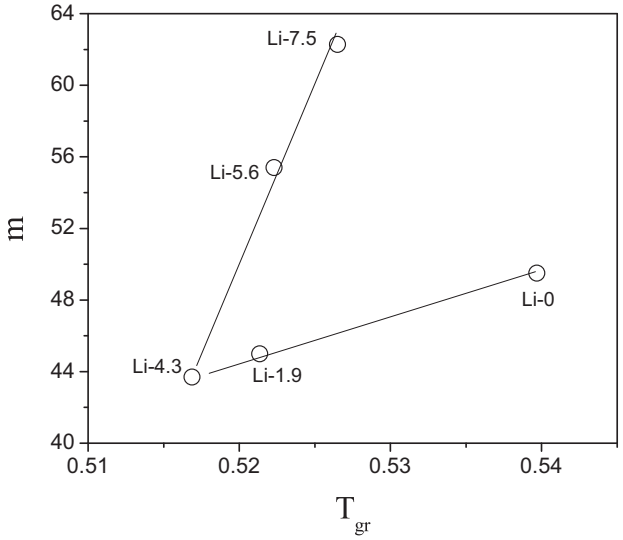


**Fig. 16.** Fragility index versus the reduced glass transition temperature. The lines are included as a guide to the eye.

nucleation rates ($I_{max}$). To a first approximation, the viscosity is responsible for the kinetic barrier for nucleation and the fragility index, which characterizes the rate of viscosity change in the glass transition range, could affect the values of $T^{I}_{max}$ and $I_{max}$. But this influence is not strong, (e.g., an increase of $m$ from approximately 43 to 62 is accompanied by a decrease in $I_{max}$ of only 8 times, see Fig. 15). Thus, our findings regarding the correlation between $m$ and $I_{max}$ did not contradict those of G. Wilde [28].

### 4.3. Crystal growth and viscosity

In addition to the thermodynamic driving force, nucleation and crystal growth are both determined by the effective diffusion coefficients ($D_\tau$ or $D_U$, respectively) of the elements that participate in the formation and further development of the crystalline phase. The $U$ and $\tau$ subindexes are designed to show that $D_U$ could generally differ from $D_\tau$ governing nucleation kinetics. As a first approximation, the Stokes–Einstein-Eyring Eq. (10) is frequently employed with viscosity to estimate the effective diffusion coefficient $D_U$ ($D_\tau$). This approximation is valid at relatively high temperatures but does not work under deep undercooling conditions $T < 1.2T_g$ (see e.g., [29,30]). Consequently, at sufficiently low temperatures, a "decoupling" occurs between the mechanisms that control viscous flow and the diffusion that determines the crystal growth. This "decoupling" is characterized by a "decoupling temperature" $T_d$. A simple way to demonstrate the "decoupling" phenomenon is to analyze a plot of $U\cdot\eta$ versus $T$. According to Eq. (12), which was derived under the assumption that $D_U = D_\eta$, the value of $U\cdot\eta$ is a weak function of temperature. Fig. 17 contains these plots of $U\cdot\eta$ versus $T$ for the Li-O and Li-7.5 glasses. Indeed, at relatively high temperatures, the value of $U\cdot\eta$ varies weakly. However, when the temperature approaches the glass transition temperature ($T_g$) it begins to increase (slowly at first and then drastically). This means that, starting from the decoupling temperature $T^U_d$, the viscosity increases more rapidly than the diffusion coefficient controlling growth decreases. The correlation between $T_g$ and $T^U_d$ ($T^U_d \approx 1.1\ T_g$) corresponds with data found in the literature because $T^U_d \approx (1.1 - 1.2)\ T_g$ (e.g., [29,30]).

The following comments can be made regarding the growth rate data in connection with the decoupling phenomenon. The $U\cdot\eta$ values at the glass transition temperature differed for the Li-0 and Li-7.5 glasses by more than one order of magnitude (see Fig. 17). At first glance, according to Eq. (12), a similarity between the $U(T_g)\cdot\eta(T_g)$ values is expected because the expression in square brackets of Eq. (12) is close to 1 under conditions of high undercooling and the value of $f\frac{k_BT}{4a^2}$ only changes weakly in the understudied temperature range. However, this expectation is only correct under the condition of equality $D_U = D_\eta$ i.e. at temperatures higher than $T^U_d$. Hence, $D_U$ must be employed rather than $D_\eta$. Consequently, the large differences between the $U\cdot\eta$ values at $T_g$ for the Li-0 and Li-7.5 glasses provide more evidence for the decoupling phenomenon, and reflect the different degrees of the deviation of $D_U$ from $D_\eta$ for the different glasses. As shown above, for the Li-0 and Li-7.5 glasses, the growth rates were measured for temperatures near $T_g$ (see Fig. 6). Based on the above observations, it would be interesting to collect and analyze the $U(T_g)$ data for several glasses with their proper fragility indexes.

### 4.4. The role of $Li_2O$ in the formation of the crystalline phase

As previously shown in Sections 3.3 and 4.2, the addition of $Li_2O$ to the $Na_2O\cdot 2CaO\cdot 3SiO_2$ glass results in a decrease in the melt viscosity and changes its temperature dependence. Together with the variation of the *liquidus*, the change of viscosity affects the maximum nucleation rate and the temperature at which it occurs.

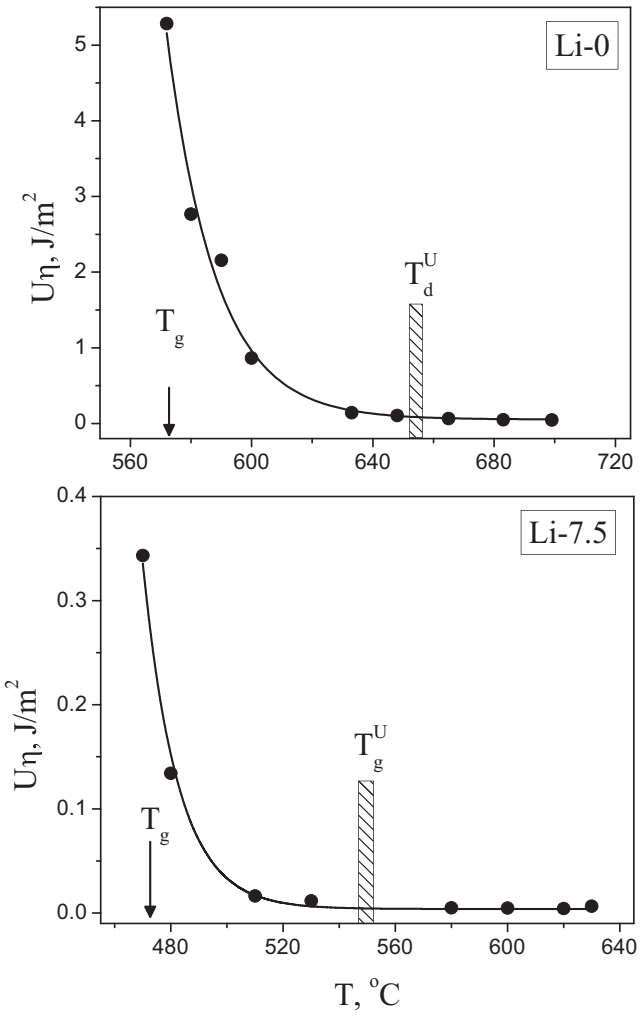


**Fig. 17.** Dependence of $U\cdot\eta$ versus temperature for the Li-0 and Li-7.5 glasses. The lines are included as a guide to the eye.

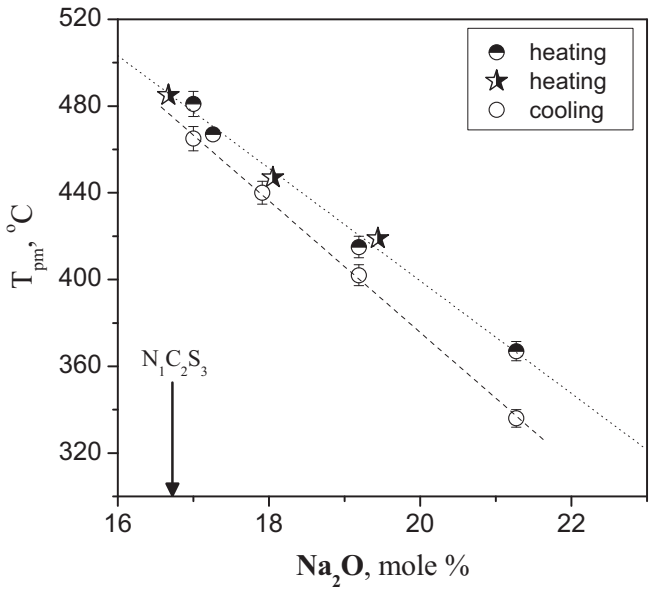


**Fig. 18.** Temperature $T_{pm}$ of the polymorphic transition from the DSC heating and cooling curves as a function of the $Na_2O$ content in the solid solution [12]. The lines are included as a guide to the eye.

In this section, we consider how the Li participates in the formation of the crystalline phases. For this purpose, we first analyzed the DSC curves. The heating curve of the Li-0 glass (i.e., glass without lithium oxide) reveals the glass transition temperature, the exothermic peak that corresponds to the crystallization of the $Na_2O{\cdot}2CaO{\cdot}3SiO_2$ phase and, finally, an endothermic peak that corresponds to the melting of this phase (Fig. 8a, curve 1). According to the $CaO{\cdot}SiO_2$–$Na_2O{\cdot}SiO_2$ phase diagram, the solid solution ($Na_{4+2x}Ca_{4-x}[Si_6O_{18}]$; $0 < x < 1$) is formed between the $Na_2O{\cdot}2CaO{\cdot}3SiO_2$ and $Na_2O{\cdot}CaO{\cdot}2SiO_2$ compounds [31]. For the present discussion, it is important that the $Na_2O{\cdot}2CaO{\cdot}3SiO_2$ crystals and its solid solution $Na_{4+2x}Ca_{4-x}[Si_6O_{18}]$ present a reversible polymorphic transition at a temperature $T_{pm}$ that is accompanied by a remarkable heat effect (see e.g., Fig. 8b, curve 1). The increase of the $Na_2O$ content in the solid solution results in a strong decrease in the $T_{pm}$ (see Fig. 18), which is accompanied by a decrease in the heat of the phase transition [12,32,33].

Let us consider the DSC curves of the $Na_2O{\cdot}2CaO{\cdot}3SiO_2$ glasses with extra $Li_2O$. The addition of $Li_2O$ results in a decrease in the glass transition temperature and the temperature of the crystallization peak (see Fig. 8a). The first addition of lithium oxide (Li-1.9) changes the shape of the melting peak, which makes it more asymmetric with the onset of a lower temperature. Regardless, it is difficult to estimate the temperature at which the first liquid appears, the expanded profile of the melting peak gives indirect evidence of the melting of a solid solution [34]. This interpretation of the melting peak will be confirmed later by using X-ray analysis. The endothermic event of the heating curve of the Li-4.3 reveals two types of processes. The first process is represented by a relatively weak endothermic peak (see the enhanced portion of the proper part of curve 3 in Fig. 8a) that corresponds to the melting of the eutectic mixture just above the temperature of the solidus, $T_S$. The area of this peak increases with increasing $Li_2O$ content (Fig. 19), indicating the direction of the eutectic point. A subsequent strongly extended endothermic event reflects the melting of a solid solution in the temperature interval between the *solidus* and *liquidus*. The final stage of this melting corresponds to the *liquidus* temperature, $T_L$. The temperatures of $T_S$ and $T_L$ with the glass transition temperature are presented in Fig. 20 as a function of the $Li_2O$ content of the parent glass. Thus, we can suppose that the fully crystallized Li-4.3 glass contains a small amount (not detectable by X-ray analysis) of the lithium-containing phase beyond the main phase (solid solution $Li_2O$ in the $Na_2O{\cdot}2CaO{\cdot}3SiO_2$ structure). Indeed, the X-ray diffraction spectra of the fully crystallized Li-5.6 and Li-7.5 glasses revealed two peaks that belong to the $Li_2O{\cdot}SiO_2$ (LS) crystals

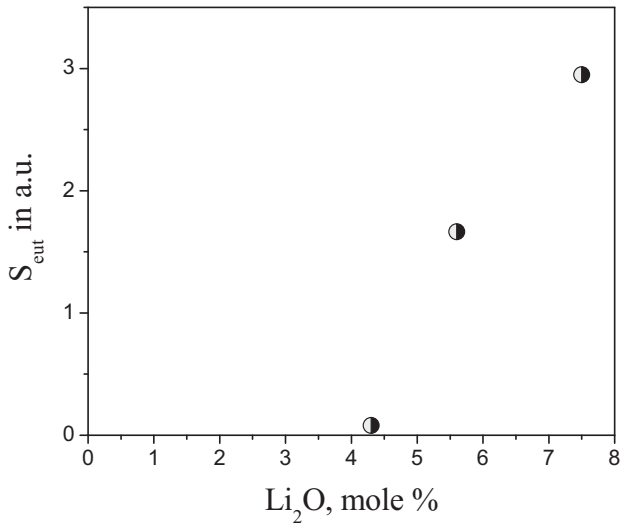


**Fig. 19.** Area of the melting peak of the eutectic mixture versus the $Li_2O$ content in the studied glasses.

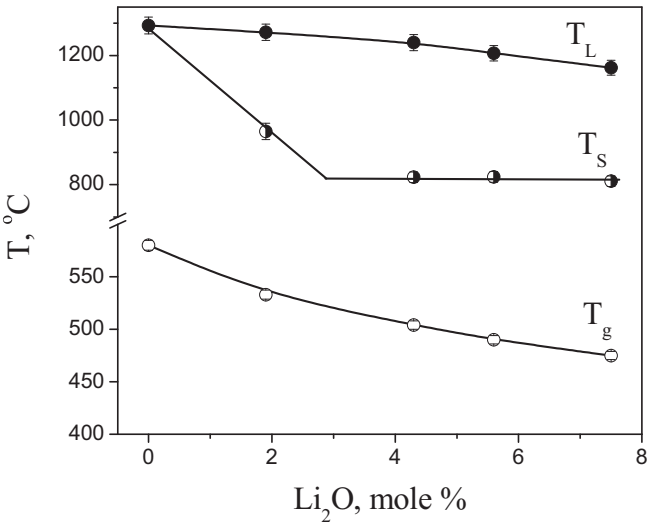


**Fig. 20.** $T_g$, $T_S$, and $T_L$ versus the $Li_2O$ contents for the studied glasses. The lines are included as a guide to the eye.

(Fig. 9) that do not match the peaks of the main $Na_2O{\cdot}2CaO{\cdot}3SiO_2$ phase. The reflected light optical micrograph and the SEM BSE image of the cross-sections of the Li-7.5 glass fully crystallized at 660 °C and 580 °C are shown in Fig. 21. The photos make it clear that the samples contain two phases. Moreover, because the BSE images are based on chemical contrast, we can attribute the dark crystals to the Li rich phase (i.e., to

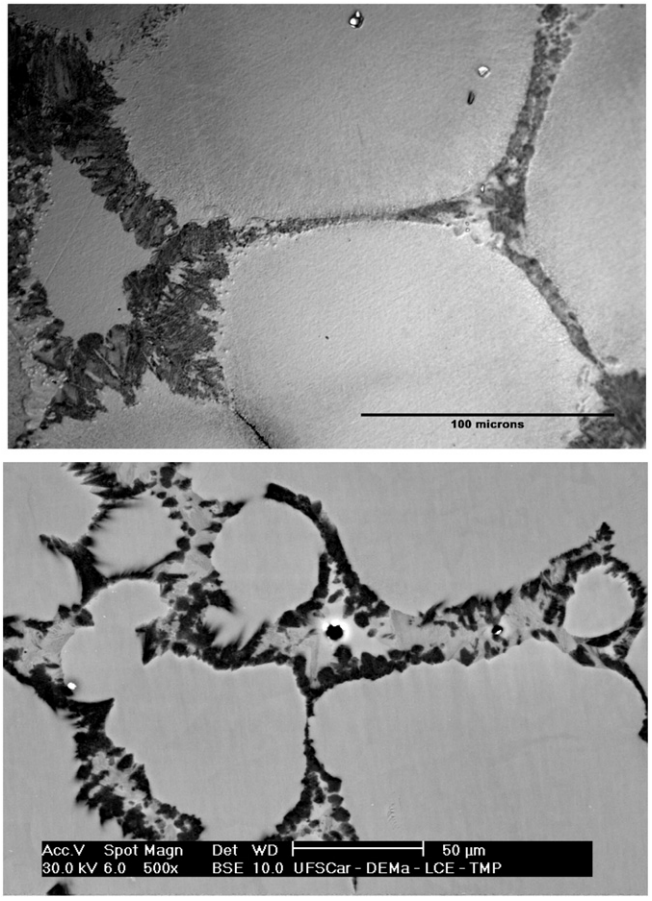


**Fig. 21.** Reflected light optical micrograph (top) and the SEM BSE image (bottom) for the cross-sections of the Li-7.5 glasses that were fully crystallized at 660 °C for 16 min and 580 °C for 8 h, respectively.

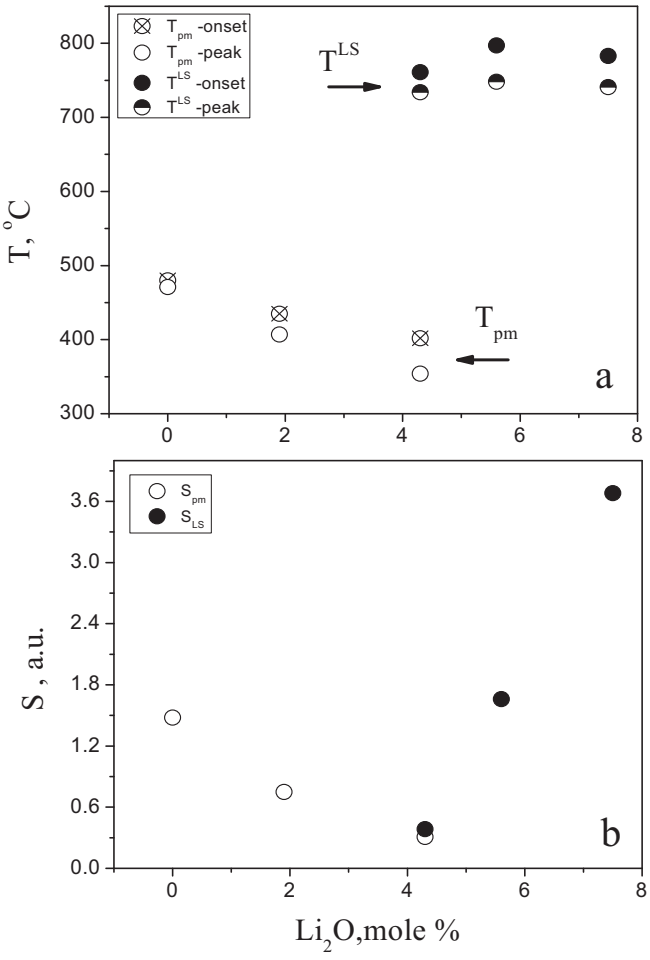


**Fig. 22.** Temperature of the solid solution polymorphic transition ($T_{pm}$) and the LS crystallization ($T^{LS}$) peaks (a) and their areas (b) versus the $Li_2O$ contents taken from the cooling DSC curves of the glasses under study.

lithium metasilicate, LS). In addition, increase of the area of the melting peak of the eutectic mix with increasing $Li_2O$ content in the parent glass (see Fig. 19) provides evidence of the increasing volume fraction of the LS crystals in the fully crystallized glasses. The crystallization of the two phases ($Li_2O{\cdot}SiO_2$ and s/s $Na_2O{\cdot}2CaO{\cdot}3SiO_2$) is also confirmed by two crystallization peaks (see zooms of curves 4 and 5 in Fig. 8a).

Besides the first (high temperature) strong exothermic peak (caused by the full crystallization of the undercooled melt), the cooling curve of the Li-1.9 reveals a second weak exothermic peak at lower temperatures (see the enhanced portion of curve 2 in Fig. 8b). This peak is caused by a reversible polymorphic transition of the solid solution. In addition, a similar peak was discussed above for curve 1 that corresponded to the Li-0 glass. Its temperature $T_{pm}$ and the corresponding area $S_{pm}$ systematically decreased as the $Li_2O$ content increased (Fig. 8b). Thus, we assumed that the Li ions were embedded in the structure of the $Na_2O{\cdot}2CaO{\cdot}3SiO_2$ crystal and formed an interstitial solid solution with limited solubility. It should be recalled that the crystal structure of $Li_2O{\cdot}2CaO{\cdot}3SiO_2$ is unknown [31]. Fig. 22 shows the temperatures (the onset and the maximum of the exothermic peak on the DSC cooling curves) of the polymorphic transition $T_{pm}$ and their areas $S_{pm}$ versus the $Li_2O$ contents beginning with the $Na_2O{\cdot}2CaO{\cdot}3SiO_2$ glass (Li-0). The values of $T_{pm}$ for the Li-1.9 and Li-4.3 glasses are approximately 407 and 354 °C, respectively. In the case of the sodium-enriched solid solution (relative to the stoichiometric composition of $Na_2O{\cdot}2CaO{\cdot}3SiO_2$), the temperatures of $T_{pm} = 407$ and 354 °C corresponded to excess $Na_2O$ concentrations of 2.2 and 4.1 mol% respectively (see Fig. 18). These values are similar to the $Li_2O$ concentrations in the Li-1.9 and Li-4.3 glasses. This result supports the assumption that Li enters into the $Na_2O{\cdot}2CaO{\cdot}3SiO_2$ crystals and results in decreased $T_{pm}$ and $S_{pm}$ values. However, it should also be considered that the fully crystallized Li-4.3 glass already contains lithium metasilicate crystals that consume $SiO_2$ from $Na_2O{\cdot}2CaO{\cdot}3SiO_2$. Thus, the structural disordering of the main phase ($N_1C_2S_3$) is first caused by the entrance of lithium and then by the loss of Si. The changes in the composition of the solid solution based on the $N_1C_2S_3$ structure (due to the loss of silica during the formation of the LS crystals) are shown in the concentration triangle (see Fig. 23).

The evolution of the crystal cell parameters with increasing $Li_2O$ content provides more information regarding the formation of the solid solution based on the $Na_2O{\cdot}2CaO{\cdot}3SiO_2$ structure. Fig. 24 shows the changes of the *a* and *c* parameters and the volume (*V*) of the hexagonal crystal cell as a function of lithium oxide content in the parent glass. According to these data, the first addition of Li (glass Li-1.9) results in a sharp decrease in *V*. This change is accompanied by changes in the melting peak shape (please see curve 2 in Fig. 8a), which are discussed above, and is interpreted as a result of the formation of a

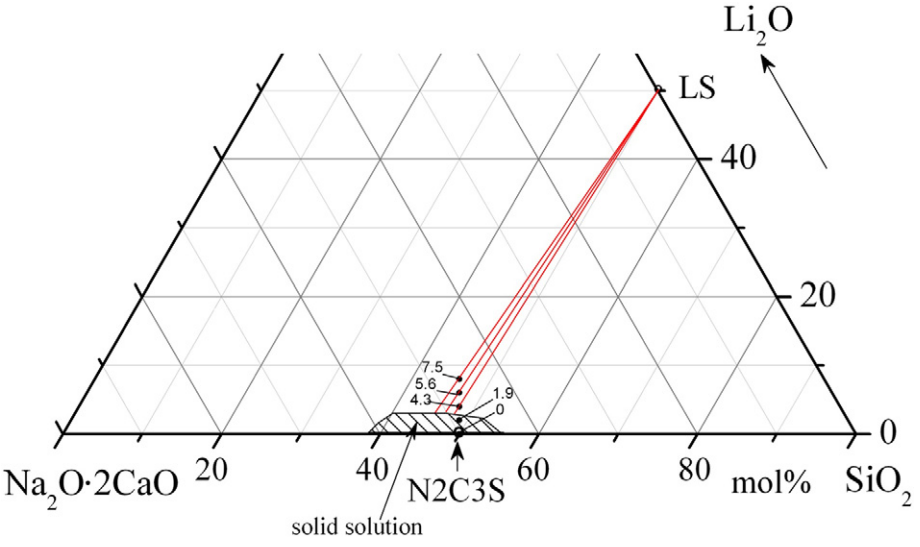


**Fig. 23.** Changes in the phase composition of completely crystallized $Na_2O{\cdot}2CaO{\cdot}3SiO_2$ glass with $Li_2O$ addition. The shaded region is a hypothetical area of the solid solutions; the black dots are the figurative points of the glasses; the numbers at the points indicate the $Li_2O$ content in the glasses; the red lines are the tie-lines which determine the decay directions under the glasses crystallization in the concentration triangle.

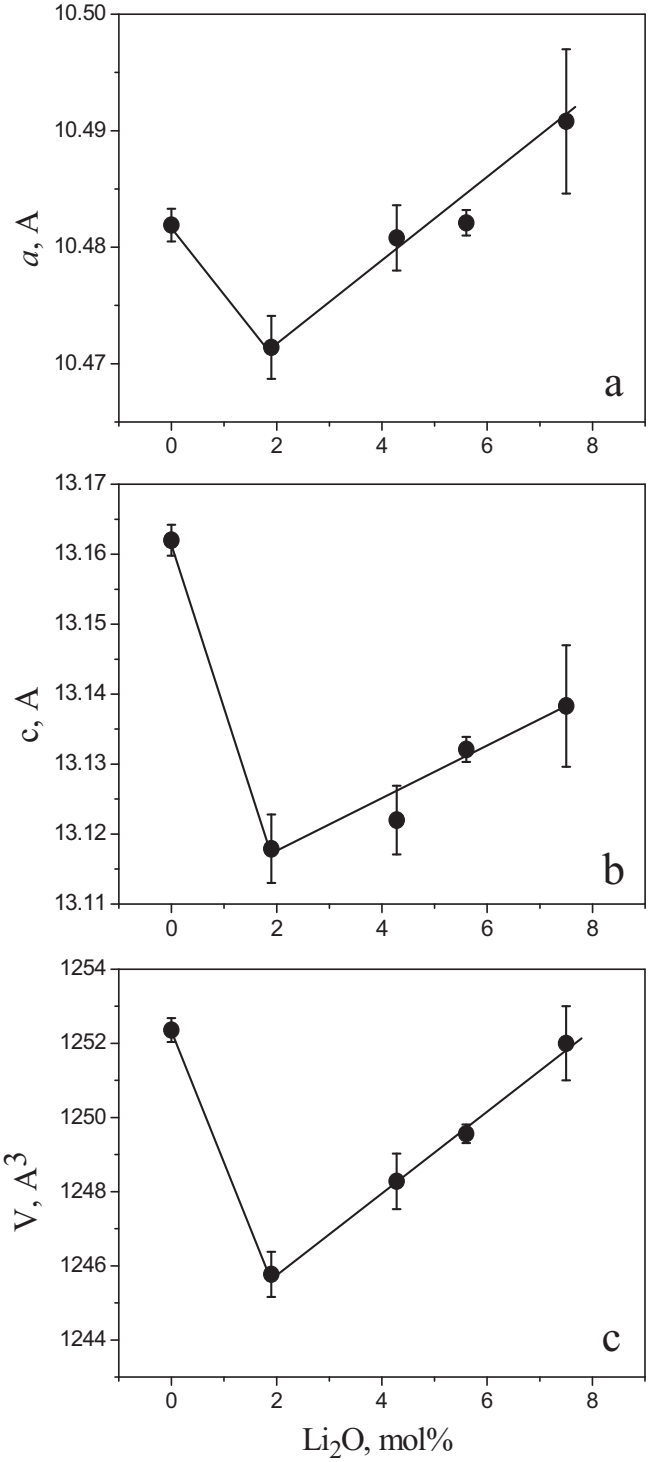


**Fig. 24.** Parameters *a* (a) and *c* (b) of the hexagonal crystal cell of the NCS crystals with cell volume *V* (c) versus the $Li_2O$ content in the parent glasses. The lines are included as a guide to the eye.

solid solution. When entering the $Na_2O{\cdot}2CaO{\cdot}3SiO_2$ structure, Li results in a smaller *V*. Furthermore, increases in the $Li_2O$ content of the parent glasses (Li-4.3; Li-5.6; Li-7.5) result in greater *V*, which could be explained by the depletion of $SiO_2$ due to the formation of lithium metasilicate.

However to confirm the above reasonable assumption, a Rietveld refinement is needed to define the atomic positions in the crystal elementary cell.

Besides the exothermic peak of $T_{pm}$, which reflects the reversible polymorphic transition of the solid solution based on the $Na_2O{\cdot}2CaO{\cdot}3SiO_2$ structure, the cooling curve for the Li-4.3 glass (Fig. 8b) reveals an exothermic peak at a higher temperature $T^{LS}$. Because the heating curve of this glass (Li-4.3) clearly shows the melting of a eutectic mixture, which reflects the appearance of lithium metasilicate (see zoom of curve 3 in Fig. 8a), we attributed this exothermic peak on the cooling curve to the lithium metasilicate crystallization. Further increases of $Li_2O$ in the parent glass result in increasing areas for this peak ($S_{LS}$) and do not change its position (see Fig. 22), which is near the solidus. According to the X-ray analysis, fully crystallized Li-5.6 and Li-7.5 glasses contain LS crystals. Moreover, the increase of this exothermic peak is accompanied by an increase in the area of the first melting peak following heating in the DSC scans (Figs. 8a, 19). This correlation provides additional indirect evidence for our assumptions regarding the origin of the second exothermic peak in the cooling curve ($T^{LS}$).

## 5. Conclusions

To investigate the crystallization pathways and kinetics of non-stoichiometric glasses thoroughly, a detailed and systematic study of the crystal nucleation and growth rates was conducted with viscosity measurements and a DSC analysis of $Na_2O{\cdot}2CaO{\cdot}3SiO_2$ glasses with additions of $Li_2O$. The main conclusions are presented below.

Additions of $Li_2O$ in the $Na_2O{\cdot}2CaO{\cdot}3SiO_2$ glasses resulted in lower viscosities and *liquidus* temperatures.

A partial section of the phase diagram of $Na_2O{\cdot}2CaO{\cdot}3SiO_2$–$Li_2O$ was constructed here via DSC analysis. It indicates a narrow range of solid solution formation, close to that of $Na_2O{\cdot}2CaO{\cdot}3SiO_2$. In the four-component system ($Na_2O$–$Li_2O$–CaO–$SiO_2$), a pseudo-binary eutectic system $N_1C_2S_3$–LS exists.

The influence of $Li_2O$ on the crystallization kinetics is mainly due to the liquidus temperature variations with the evolution of the melt viscosity. With increasing $Li_2O$ content in the parent glasses, the fragility index and the reduced glass transition temperature exhibit a minimum. The compositions of these minima are similar to the composition of the glass that reveals the highest nucleation rate, $I_{max}$. These findings extend and confirm the previously determined correlation between $T_{gr}$ and $I_{max}$ (the lower the $T_{gr}$ the higher is $I_{max}$) and provide evidence for a similar correlation between *m* and $I_{max}$.

At temperatures far below the liquidus, the crystal growth rates increase as the $Li_2O$ content increases. An analysis of the temperature dependence of the crystal growth rates shows a decoupling between the effective diffusion coefficients that govern the crystal growth, U, and viscosity, η, at $T < 1.1T_g$. This phenomenon has been reported before for various stoichiometric glasses. Finally, the value of the $U{\cdot}\eta$ product at $T_g$ is suggested as a parameter for characterizing the decoupling phenomenon. Overall, these results provide new insights regarding the crystallization of non-stoichiometric glasses.

## Acknowledgements

The authors thank the Brazilian funding agencies CNPq and FAPESP — the São Paulo Research Foundation — CEPID process # 2013/07793-6.

## References

[1] W. Hölland, G. Beall, Glass-ceramic Technology, Wiley — American Ceramic Society, Hoboken, NY, 2002.
[2] I. Gutzow, J. Schmelzer, The Vitreous State: Thermodynamics, Structure, Rheology and Crystallization, Springer, Berlin, 1995.
[3] G.P. Souza, V.M. Fokin, E.D. Zanotto, J. Lumeau, L. Glebova, L.B. Glebov, Phys. Chem. Glasses Eur. J. Glass Sci. Technol. B 50 (2009) 311.
[4] I. Dyamant, A.S. Abyzov, V.M. Fokin, E.D. Zanotto, J. Lumeau, L.N. Glebova, L.B. Glebov, J. Non-Cryst. Solids 378 (2013) 115.
[5] V.M. Fokin, E.D. Zanotto, J.W.P. Schmelzer, J. Non-Cryst. Solids 321 (2003) 52.
[6] V. Guencheva, C. Rüssel, V.M. Fokin, I. Gutzov, Eur. J. Glass Sci. Technol. 48 (2007) 48.
[7] J. Deubener, J. Non-Cryst. Solids 274 (2000) 195.
[8] K. Thieme, C. Rüssel, J. Eur. Ceram. Soc. 34 (2014) 3969.

[9] C.J.R. Gonzalez-Oliver, P.F. James, J. Non-Cryst. Solids 38&39 (1980) 699.
[10] V.M. Fokin, O.V. Potapov, E.D. Zanotto, F.M. Spiandorello, V.L. Ugolkov, B.Z. Pevzner, J. Non-Cryst. Solids 331 (2003) 240.
[11] A.C.M. Rodrigues, G.T. Niitsu, E.D. Zanotto, M.O. Prado, V. Fokin, J. Non-Cryst. Solids 353 (2007) 2237.
[12] V.M. Fokin, E.D. Zanotto, J. Non-Cryst. Solids 353 (2007) 2459.
[13] T. Berthier, V.M. Fokin, E.D. Zanotto, J. Non-Cryst. Solids 354 (2008) 1721.
[14] O. Peitl, PhD thesis, Universidade Federal de São Carlos, 1995.
[15] M.L.G. Leite, PhD thesis, Universidade Federal de São Carlos, 2001.
[16] V.M. Fokin, E.D. Zanotto, N.S. Yuritsyn, J.W.P. Schmelzer, J. Non-Cryst. Solids 352 (2006) 2681.
[17] O.V. Potapov, V.M. Fokin, V.L. Ugolkov, L.Y. Suslova, V.N. Filipovich, Glas. Phys. Chem. 26 (2000) 39.
[18] C.V. Thompson, F. Spaepen, Acta Metall. 31 (1983) 2021.
[19] D. Kashchiev, Surf. Sci. 14 (1969) 209.
[20] J. Frenkel, Kinetic Theory of Liquids, OxfordUniversity Press, Oxford, 1946.
[21] K.A. Jackson, Kinetic Processes, WILEY-VCH, Weinheim, 2004.
[22] C. Kroger, G. Kreitlow, Glastechn. Ber. 29 (1956) 393.
[23] V.M. Fokin, E.D. Zanotto, J.W.P. Schmelzer, J. Non-Cryst. Solids 278 (2000) 24.
[24] J.W. Christian, Theory of Transformations in Metals and Alloys. Part I, Pergamon Press, Oxford, 1981.
[25] V.M. Fokin, M.L.F. Nascimento, E.D. Zanotto, J. Non-Cryst. Solids 351 (2005) 789.
[26] J. Orava, A.L. Greer, J. Chem. Phys. 140 (2014) 214504.
[27] C.A. Angell, J. Phys. Chem. Solids 49 (1988) 863.
[28] G. Wilde, Early Stages of Crystal Formation in Glass-forming Metallic Alloys, in: J.W.P. Schmelzer (Ed.), Glass, De Gruyter, 2014.
[29] M.L.F. Nascimento, V.M. Fokin, E.D. Zanotto, A.S. Abyzov, J. Chem. Phys. 135 (2011) 194703.
[30] M.L.F. Nascimento, E.D. Zanotto, J. Chem. Phys. 133 (2010) 174701.
[31] A.R. West, J. Am. Ceram. Soc. 61 (1978) 152.
[32] G.K. Moir, F.P. Glasser, Phys. Chem. Glasses 15 (1974) 6.
[33] I. Maki, T. Sugimura, J. Ceram. Assoc. Jpn. 76 (1968) 144.
[34] I.G. Polyakova, E.N. Tokareva, Glas. Phys. Chem. 23 (1997) 354.